Chitosan gel film bandages: correlating structure, composition and antimicrobial properties

P. Anaya[1]*, G. Cárdenas[2], V. Lavayen[3], A. García[4], and C. O'Dwyer[5]*

[1] *Departamento de Ciencias Básicas, Escuela de Educación–Campus Los Ángeles, Universidad de Concepción, Los Ángeles, Chile*

[2] *Laboratorio de Materiales Avanzados (CIPA), Departamento de Polímeros, Facultad de Ciencias Químicas, Universidad de Concepción, Concepción, Chile,*

[3] *Pontifícia Universidade Católica do Rio Grande do Sul, Faculdade de Química/PGETEMA, P.O. Box 1429, CEP 90619-900, Porto Alegre, Brazil*

[4] *Departamento de Microbiología, Facultad de Ciencias Biológicas, Universidad de Concepción, Concepción, Chile*

[5] *Applied Nanoscience Group, Department of Chemistry, and Tyndall National Institute, University College Cork, Cork, Ireland*

* To whom correspondence should be addressed: Email: panaya@udec.cl;

Email: c.odwyer@ucc.ie; Tel: 00 353 21 4902732; Fax: 00 353 21 4274097

KEYWORDS: polymer, bandage, chitosan, antibacterial, antimicrobial

Abstract

Chitosan gel films were successfully evaporation cast from chitosan solutions in aqueous acidic solutions of organic acids (lactic and acetic acid) as gel film bandages, with a range of additives that directly influence film morphology and porosity. We show that the structure and composition of a wide range of 128 thin gel films, is correlated to the antimicrobial properties, their biocompatibility and resistance to biodegradation. Infrared spectroscopy and solid-state ^{13}C nuclear magnetic resonance spectroscopy was used to correlate film molecular structure and composition to good antimicrobial properties against 10 of the most prevalent Gram positive and Gram negative bacteria. Chitosan gel films reduce the number of colonies after 24 hours of incubation by factors of ~10^5 – 10^7 CFU/mL, compared to controls. For each of these films, the structure and preparation condition has a direct relationship to antimicrobial activity and effectiveness. These gel film bandages also show excellent stability against biodegradation with lysozyme under physiological conditions (5% weight loss over a period of 1 month, 2% in the first week), allowing use during the entire healing process. These chitosan thin films and subsequent derivatives hold potential as low-cost, dissolvable bandages or second-skin, with antimicrobial properties that militate against the most relevant intra-hospital bacteria that infest burn injuries.

Introduction

Chitosan, formed by a mixture of β-(1,4)-D-N-acetylglucosamine and β-(1,4)-D-glucosamine, is an exceptionally useful polysaccharide derived from deacetylation of chitin, which is found in the cell walls of lower plants and in the exo-skeletal tissues of lower animals including arthropods, crustaceans, and molluscs[1, 2]. Exploiting the high molecular weight of chitosan gives it the ability to form polymeric gel-like films[3] by evaporation casting, layer-by-layer growth[4], or by addition of plasticizers. There have been several investigations into the antimicrobial activity of chitosan and its derivatives[5-7]. One of the suppositions is that the cationic property of chitosan allows it to interact with the negative residues of the cellular wall and alter the permeability causing the cell to lose proteins and intracellular electrolytes[7-11]. As a functional polymer, it has several distinctive biomedical properties such as low toxicity, negligible cytotoxicity, biocompatibility and biodegradability[12]. One property of chitosan is its ability to rapidly clot blood, and has recently gained approval in the United States and Europe for use in bandages and other hemostatic agents. The enzymatic degradation of chitosan is one of its advantages in preparing various materials for medical purposes, such as films, sutures, coatings and gels[12].

Chitosan is currently receiving a great deal of interest for medical and pharmaceutical applications. Due to promising biocompatibility effects, topical ocular applications are possible, as well implantation or injection uses. Biologically, chitin and chitosan provide sources of glucosamine, a potentiator for antibiotics and consequently a substance with wound-healing properties. Chitosan is a hemostatic, and it also promotes collagen formation, thus helping to reduce scar formation. The chemistry and mechanical properties of chitosan also gives it excellent film forming and handling properties, and it has great utility in the formation of

membranes[13]. Its toughness can be utilized in producing high strength fibers and bioseparation films and it therefore may have other medical applications such as sutures. Furthermore, chitosan is metabolized by certain human enzymes, *e.g.* lysozyme, and can be considered as biodegradable[12, 14]. Medical applications of chitosan composite gel films performed on patients with burns, ulcers and injuries have shown that films containing glycerol exhibit good adhesion and elasticity in comparison with those without. We previously showed excellent performance[8] in skin recovery after 7–10 days from patients with various degrees of burn injury, using chitosan acetate and lactate. Complete epithelialization was observed in the patients treated with the gel films[8] and subsequent full healing occurring using these 'second skin' bandages.

In severe burns, the complete thickness of the skin can be destroyed and the definitive standard solution is an autologous graft. Surgeons often use temporary grafts or 'second skin' cover materials to prevent infections[15]. Colonization of burn wounds by microorganisms due to the presence of bacteria in necrotic tissue of an open injury is generally established during the first week. The infection is promoted by the loss of the epithelial barrier, the malnutrition induced by the associated hypermetabolic response, and also because of immune suppression, due to the release of immunoactive agents from the injury. Pathogen bacteria infection occurs then within the first 10 days. The burn scar vascularization is natural part of the healing process, but openings quickly allow colonization by micro-organisms and bacteria, even with the use of antimicrobial agents. Chitosan, and its derivatives in film form, allow total coverage of the wound in addition to proving antimicrobial support during healing. The chitosan was found to be biodegradable by enzymes present during healing wounds and the gel film does not need to be removed preventing dehydration and infection; an improvement in the gradual growth of damaged tissues was possible.

Here, we report the formation of novel chitosan gel films achieved by evaporation casting on several solvents such as acetic and lactic acid solutions, their biodegradation properties in lysozyme, and the antimicrobial properties of the chitosan films against 10 of the most prevalent Gram positive and Gram negative bacteria responsible for many intra-hospital infections. Detailed spectroscopic (solid state cross polarization magic angle spinning NMR, IR) investigations into the structural properties and interactions of the polymeric macromolecules, correlate the polymeric structure to antimicrobial properties and biodegredation. These chitosan films can be structurally and compositionally tuned with physical properties that have beneficial antimicrobial and biodegradation effects, slated for development as low-cost, dissolvable bandages, or transparent and protective 'second skin' patches, against the most relevant intra-hospital bacteria that infest burn injuries.

Materials and methods

Chemicals and reagents

Two varieties of chitosan from shrimps (Pleuroncodes monodon), provided by Quitoquimica Ldta, were used for chitosan acetate film preparation. The molecular weight was calculated from the dependence on the polymer intrinsic viscosity [η] using the Mark-Houwink relation[16], $[\eta] = KM^a$, where $K = 0.076$ and $a = 0.76$. For chitosan the K and a values are strongly dependent on the degree of deacetylation. The deacetylation degree in both compounds was around 97% and the low, medium and high molecular weights used were determined to be 68, 138 and 263 kg mol^{-1}, respectively. The deacetylation degree was determined by potentiometric titration. The acid–base titration of the $NH_3^+Cl^-$ from chitosan was carried in a known excess of 0.1 N NaOH. A pH meter WTW pH 531, with a combined glass electrode WTW Sen Tix 41, pH 0–14/0–80 °C

is used and the change in pH due to neutralization with the advance of reaction is followed. Egg white lysozyme was purchased from Sigma Aldrich Chemical Co. All the reagents for the studies were analytical grade. Clinically isolated bacterial strains used for the antimicrobial test were provided by Hospital del Trabajador, Chile. American Type Culture Collection (ATCC) strains came from the microbiology bank of the Faculty of Biological Science, Chile.

Film preparation

Chitosan films were obtained by evaporation casting with organic acid solutions such as acetic and lactic acids, and also with different additives such as glycerol, fatty acids, and their mixtures. the composition of the solutions were carefully controlled and excesses in organic solutions were removed. The pH of each film formation solution was adjusted with a 5% solution of NaOH and maintained at 5.4. The films were obtained from 25 mL of filtrated final mixture were placed in Petri dishes and placed in a Shell lab 14-2 oven with air convection at 36 °C for 12 hours until complete film formation. Excess salts are subsequently removed and excess glycerol is removed prior to investigations of the gel swelling. Table 1 shows the variables (solutions, additives etc.) used for the assays. The principal factors were maintained in all experimental designs, while the secondary factors were used to tune and differentiate results between conditions with the aim of determining the best combination set.

The independent main variables during tests, summarized in Tables 1 and 2, (I) chitosan molecular weight, (II) percentage of chitosan, (III) type of solvent and (IV) glycerol in the solution, respectively. The secondary variables were additives such as (V) oleic, (VI) linoleic acids and (VII) polyoxyethylenesorbitan monolaureate (Tween 20) and (VIII) polyoxyethylenesorbitan monooleate (Tween 80) surfactant concentrations, with a total of 128

different films obtained and examined. Swelling in glucose and saline solutions for several films was evaluated, and swelling is found to be higher in the glucose solutions. Additionally, porosity within the films is important for oxygen permeability which was achieved with these composites by forming an aerogel prior to casting. Thin films of optically transparent chitosan have been investigated in addition to its biomimetic properties[13, 17]. Their direct conversion to films, that exhibit controllably different physical and antimicrobial properties that depend on the additives used, their mixture and resulting film thickness gives possibilities for mouldable thin film applications.[18]

Film characterization

Thickness of films from the Experimental Design A set was in the range of 0.023 – 0.046 mm ± 0.004 mm, measured with an Electronic Digital Micrometer from Vetto & Co., USA with a resolution of 1 μm. Different amounts of additives for each Experimental design were tested in order to obtain the best films for biological property assessment, determined to be those with a 1% chitosan concentration. Thickness measurements and film morphology for representative films were also investigated using scanning electron microscopy (SEM) in a JEOL JSM 6380LV. Samples were sputtered with 15 nm of gold to minimize e-beam charging of the films.

Optical spectroscopy of chitosan gel films

The chitosan films were examined using Fourier transform infra-red spectroscopy and spectroscopic ellipsometry. The vibrational IR spectra of the composites were recorded with a 2 cm^{-1} resolution in a Nicolet Nexus spectrophotometer. Small coupons of cast films were used in a NaCl window with no previous treatment. Since cast films were prepared at 36 °C,

contributions from water molecules in films were taken into account for quantitative analysis. Refractive indices of the films with known thickness were independently determined using a M-2000UTM Spectroscopic Ellipsometer, (J. A. Wollam Co., Inc) in the wavelength range 400 – 900 nm.

^{13}C cross-polarization magic angle spinning solid state nuclear magnetic resonance (^{13}C CP-MAS NMR)

The room temperature ^{13}C CP-MAS NMR characterization of the solid material was performed using a Bruker CXP 300 spectrometer with 3000 accumulations at a spinning frequency of 5.7 kHz and a contact time of 2 ms using a broadband CP-MAS probe. Recycle delays were typically between 5 and 10 s and 4,4-dimethyl-4-silapentane-1-sulfonic acid (DSS) was used as a reference.

Antimicrobial assay

The antimicrobial activity of the films was measured primarily by the diffusion disc method or Kirby–Bauer method in order to determine the leaching of the respective antimicrobial principle. Composite discs of Ø = 1 cm were placed on the nutrient solid media containing the microorganism to assay. In the second part of the study, the dynamic contact method described by ASTM E 2149-01[19] was used to quantify the antibacterial characteristics of the material using small pieces of film immersed in bacterial culture with a concentration of 10^5 – 10^6 CFU/mL (ASTM E 2149–01). Table 3 lists the 10 microorganisms investigated in the assays.

In vitro biodegradation assay

The *in vitro* biodegradation of the films was measured under physiological conditions in a phosphate buffered solution. Films prepared on discs of 1 cm diameter were immersed for a duration of 28 days in the solution containing lysozyme at bodily fluid concentrations at 36 °C. Two different concentrations of enzyme were used: C1 = 1.5 μg/mL and C2 = 1 mg/mL.

Results and discussion

Evaporation cast chitosan films have macroscale (1-100 μm) morphologies similar to cellophane and commercial polypropylenes, as shown in Fig. 1a. SEM examination of the surface and cross-sections in Fig. 1c-e show that the additives outlined in Table 1 gave a plasticizing effect and the resulting morphology the gel films was smooth but contains pores that run through the thickness of the film from the top surface. The addition of glycerol and Tween 80 for example, changes the characteristic surface topology, but maintained a coherent film with minimal cracking. The surface of Ø = 1 cm chitosan discs used during assays (see below) was also found to be smooth but partially porous as evidenced by the differential interference contrast optical image in Fig. 1b, where a limited number of super-wavelength roughness features are seen[20]. The porosity in the chitosan composite mixtures during gelation and plasticizing allows oxygen permeation through a wound dressing which maintains the healing rate and also the proliferation of anaerobic bacteria.

AFM measurements of surface roughness confirm that the additives, such as glycerol, give a more homogeneous, non-porous surface due to its plasticizing effect; all additives in these series of films affect roughness with the highest influence on morphology caused by the solvent. For the smoothest, most uniform films, we characterize and relate the differences in composition

and structure (both morphology and chemical structure) to their antimicrobial and biodegradation properties.

FTIR and ^{13}C CP-MAS NMR characterization of chitosan gel films

Representative samples from each experimental design underwent spectroscopic characterization to determine the chitosan state (powder or gel film) by examining organic contributions and their interaction, by monitoring changes in the line-shape and frequency shift of the molecular vibrations[21]. FTIR spectra acquired from a chitosan solution in acetic acid without any additive, chitosan powder, and two representative chitosan films, are shown in Figs 2a and 2b. From 1400 to 1700 cm^{-1} in all samples, we find signals at 1656 cm^{-1} corresponding to the stretching of carbonyl group (C=O), and at 1598 cm^{-1} from the deformation mode of the free amino group NH_2[21]. For the chitosan solution in acetic acid, axial vibrations of the carboxylate anion (COO^-) confirm chitosan salt formation.

In the region 3000 – 3700 cm^{-1} (Figs 2a and 2b), all forms of the chitosan studied in this work exhibit this band corresponding to OH stretching from hydration. The characteristic OH band overlapped by the NH stretching at ~3400 cm^{-1} from the chitosan powder is routinely observed to shift to lower frequencies when cast as a film due to an increased water content in the film structure. Separated signals of the OH groups at 3458 cm^{-1} and the NH band at ~3300 cm^{-1} confirm the reaction between the OH from chitosan and the acetic acid to form the ester group. The characteristic band of CH_2 scissoring at 1420 cm^{-1} from the chitosan are found to shift to lower frequencies for the films due to the rearrangement of the hydrogen bonds[22], detailed in Table 4.

In addition, at 1581 cm^{-1} a vibration from N-H is observed, due to the unprotonated amino group (symmetric stretching N-H)[23-25]. This specific coordination vibration was also observed only in samples numbered *1035*, *2021*, *8021*. No vibrational contributions from the amino salt group (NH_3^+) were observed for all samples investigated. The bending mode from CH_2 groups at 1432 cm^{-1}, and CH_3 groups at 1379 cm^{-1} in chitosan are blue-shifted to 1400 cm^{-1} in its polymeric derivative.

Figure 2b shows the FT-IR spectra for two Experimental Design A composites: *1001* (from acetic solution – chitosan acetate) and *1043* (from lactic solution – chitosan lactate). The presence of additives and also the solvent is observed from the IR signature. For instance, for sample *1043* prepared from lactic acid solution, the band from stretching of the carbonyl group (C=O) is found at 1728 cm^{-1} and the stretching of the simple C-O bond found between 1149 cm^{-1} and 1018 cm^{-1}; these vibrations confirm the formation of the chitosan lactate[26, 27]. The absorption bands observed at 1635 and 1603 cm^{-1} in pure chitosan are significantly changed in the spectra of their corresponding films. Bands attributed to C=O stretch (amide II) are shifted to lower frequency (1643 and 1557 cm^{-1}) with respect to chitosan (Table 4) in those containing acetic acid, due to acetate presence. Films cast from lactic acid still contain chitosan lactate salt due to the lower volatility of lactic acid and it is these salts that contribute to the carboxyl presence detected using IR. The spectral bands confirm the presence of the additives (acids, double bonds), and salt formation in the case of acetates or lactates. All gel films evaporation cast from solutions with lactic acid exhibit a band from C=O group stretching at 1730 cm^{-1} in addition to C-C(C=O)-C mode stretches centered at 1250 cm^{-1} and O-C-C stretching at 1140 cm^{-1}. These modes indicate the presence of chitosan lactate films, which is a critical step in the formation of antimicrobial films, as detailed further on.

The degree of substitution (DOS) and degree of amidation for all composites studied were also determined through peak area integration and ratio factoring using FTIR data, in parallel with ^{1}H NMR analyses. As the degree of chitosan substitution increases, the relative intensity of the amide I band represented in the IR spectra by the NH-CO-R (~1657 cm^{-1}) stretch, is found to increase. The following fingerprint trends are found: at lower degrees of substitution, the amide I mode appears as a shoulder, whereas at a higher degree of substitution, it is a well-defined band which overlaps with the amide I band from C=O vibrations (1650 cm^{-1}) of acetyl groups in the chitosan.

^{13}C cross-polarization magic-angle spinning nuclear magnetic resonance (CP-MAS NMR) spectra were acquired to probe the coordination and polymeric interactions within the large set of chitosan gels. A representative spectrum from the chitosan acetate-based gel film *1001* is shown in Fig. 3, and the chemical shifts of the chitosan gels films compared with previous reports from chitosan salts are given in Table 5. All spectra from the gels show the characteristic signals from chitosan, in addition to the prominent presence of carbonyl and methyl groups at 180 ppm and 24 ppm[22,23], respectively, from the carboxylic acids[23] used as solvents[24,25]. Resonance at δ = 174.6 ppm related to N-acetyl glucosamine units is observed in the spectra from gels, close to the resonance at 180 ppm which comes from carbonyl carbon from the carboxylate group[26]. The ^{13}C CP-MAS NMR spectrum of gel *1001* obtained from chitosan solution in acetic acid with glycerol as an additive, shows resonances of δ = 25 ppm in the spectrum, assigned to the CH_3 carbon.

At δ = 105 ppm there is a small resonance from the anomeric carbon atom of acetylated units, and no observable splitting of the resonance due to the anomeric C atom from γ-gauche conformations (~98 ppm) is found in the films' spectra. NMR signals from chitosan in the films

are observed with resonance bands (see Fig. 3) at δ = 104.7 (C4), δ = 85 (C3), δ = 74 (C5), δ = 60 (C6), δ = 56 (C2), and summarized in Table 2, Supporting Information for other films. Resonances at δ = 162.5 (C7, carbonyl carbon on the acetyl group), and δ = 12.8 (C8, methyl carbon on the acetyl group) are not observed in the films (Fig. 3 and Supporting Information). A very low intensity, broad peak from the film at ~120 ppm corresponds to remnant C=C bond presence. This signal represents the amount of carbon-carbon double bond conversion, a significant presence of which is known to result in increased cytotoxicity[33]. At δ = 131.5 (C1) ppm, cross-linking with amino group during chitosan film formation is found[34]. The analysis confirms that the chitosan films made using acetic and lactic acids as a dissolving vehicle formed the corresponding acetic or lactic salt[35] and its degree of formation. Overall, spectroscopic characterization of the composites, probing organic phases and interactions, showed the characteristic formation of chitosan salt when an organic acid was employed as a solvent in the presence of additives.

Antimicrobial and biodegradation properties of chitosan gel films

Antimicrobial studies of the chitosan films against the Gram positive and Gram negative microorganisms summarised in Table 2 were also conducted. Figure 4 shows the percentage increase in disc diameter measured from each of the diffusion disc assays. The microorganisms are not observed to grow under the swollen film. As a result, the contact area with the microorganism shows an inhibition of its growth in tandem with an increase is disc diameter. In a few cases, we observed areas where there is negligible film growth even in the presence of microorganisms, which contradicts recent findings[34, 36, 37] that report much higher (~98%) halo inhibition from films cast from solutions with a different pH. The investigation has also found

that the antimicrobial activity is limited or in some cases, not at all evident under certain preparatory conditions where the temperature exceeds 36 °C that result in dried thin films, as has been suggested for related chitin-derivatives[38]. The films here maintain a hydrated gel-like morphology with consistent thickness and refractive index of 1.54 determined by spectroscopic ellipsometry.

The dynamic contact method used for the second part of the antimicrobial studies demonstrated that almost all films prepared have antimicrobial activity, whose effectiveness depends on the preparation of the film, and thus its molecular structure. As shown in Table 3, almost all films reduce the number of colonies after 24 hours of incubation by factors of ~10^5 – 10^7 CFU/mL, compared to controls. For each of these films, the film structure and preparation condition has a direct relationship to antimicrobial activity and effectiveness. Careful re-examination of ghost films shows that the antimicrobial efficacy is due to the chitosan and not from any residual acids or additives used in fabricating the films. The films were also assessed for biodegradability in the light of their use as bandages and wound-healers. In spite of the lack of FDA approval for chitosan, its potential for wound healing, controlled biodegradation and drug delivery is promising[39,40]. Chitosan can be degraded *in vitro* by lysozyme[41] and its rate of degradation is inversely proportional to the degree of deacetylation[42, 43]. NMR data in Fig. 2 and Supporting Information confirmed acetylated units along the molecular chain.

The *in vitro* biodegradability of the films with lysozyme under physiological conditions at 37 °C showed, for several concentrations of enzyme, that the standardized weight loss (accounting for solubilized water-soluble additives) of the chitosan films approached 10% (90% of the initial weight of the disc). Figure 5 shows the standardized weight loss of chitosan films. It

is found that the films lose a maximum of 10% of their weight over 1 month[44], confirming good resistance to biodegradation over periods of project use as antimicrobial burn-wound bandages.

The film *1001* that contains glycerol as an additive shows the greatest weight loss due to biodegradation in comparison with films that have secondary additives. This film is an acetate and a corresponding lactate (*1035*) shows greater biodegradation in the same timeframe most probably due to the less ordered, cracked morphology of the film as seen by SEM (Supporting Information Fig. S1. Consequently, samples labelled *1050* and *1058* from Experimental Design A showed 80% less weight loss than the *1001* film, due to the addition of oleic and linoleic acid, respectively, to the acetate. Composites 2017 and 2021 from Experimental Design C series, lost only ~5% of their weight over a period of a month with just ~2% loss over the first week and gave the best antimicrobial response as seen in Table 3.

Sample 8021 from Experimental Design C series (*cf.* Table 1) degrades with a similar rate to other gel film series for the first 7 days, however due to the beneficial action of hydroxyl groups from the glycerol additives, biodegradation is slowed from 7 – 20 days and eventually reaches a maximum of only ~4% total weight loss after 1 month. Indeed, for most films, the maximum biodegradation rate occurs within the first 7 days, with the composite remaining stable for 28 days without further significant weight loss. Examination of this process over the duration of analysis by intermittent IR spectroscopy showed that there was negligible blending of agents leaching from the gel films. The biodegradation resistance is similar to photo-polymerized, cross-linked methacrylated glycol chitosan. Even though cross-linking is observed through CP-MAS NMR spectra, and considering that lysozyme should be more accessible to the polymer backbone through binding 6 sugar rings[45] in less cross-linked polymers, the measured biodegradation is quite low. Characteristically, for the majority of gel film samples from all three

experimental designs, the maximum biodegradation measured as a weight loss occurs within the first 2 weeks and stable for the following 2 weeks.

Conclusions

A wide range of chitosan-based gel films have been successfully prepared by evaporation casting as functional bandages. Depending on the preparation condition, which includes mixtures of solvents and additives, chitosan gel films can be tuned with physical properties that have beneficial bactericidal and antimicrobial effects in the control of the most relevant intra hospital bacteria that infest burn injuries. The correlation between preparation and resulting molecular structure was achieved through microscopy and spectroscopy investigations of the gel films and linked specifically to corresponding antimicrobial performance. Gel films exhibit different physical properties and macromolecular structure depending on the additives used, their mixture, degrees of deacetylation, substitution and amidation.

The final biomaterial morphology and composition dependence of these films on the antimicrobial activity; films that undergo less biodegradation are acetates or lactates, smoothened by the choice of solvent and plasticizing additives to prevent cracking and porosity. Specifically, the corresponding antibacterial activity showed a relative dependence on the chitosan molecular weight, quantity and solvent and typically allows a reduction in the number of colonies after 24 hours of incubation by factors of ~10^5 – 10^7 CFU/mL, compared to controls for some Gram positive and Gram negative bacteria. Since chitosan is a biomaterial already used in various medical devices and holds considerable potential in the fields of regenerative medicine and tissue engineering. In tandem with its resistance to biodegradation, gives a useful biopolymer while acknowledging the trade-off between resistance to enzymatic degradation and antimicrobial

efficacy. When cast as thin gel films which are capable of being moulded to bandages or ‘second skin patches’ for burn-wound recovery.

Acknowledgments

The authors would like to thank the financial support from INNOVA BIO-BIO (Grant 03-B1-212-L1), and the collaboration from The Microbiology Department, Universidad de Concepción. P. A. is grateful to the Hospital del Trabajador, Concepción, Chile for providing ATCC clinically isolated strains. V.L. thanks the projects CNPq, Brazil (400297/2010-8), FONDECyT (1090683, 1090282), and PBCT grant ACT027, Chile. Part of this work was conducted under the framework of the INSPIRE programme, funded by the Irish Government’s Programme for Research in Third Level Institutions, Cycle 4, National Development Plan 2007-2013. This work was also supported by Science Foundation Ireland under contract no. 07/SK/B1232a.

References

1. R. A. A. Muzzarelli and M. G. Peter, *Chitin Handbook*, Atec, Grottammare, Italy, 1997.
2. D. Raafat and H. G. Sahl, *Microbial Biotech.*, **2009**, *2*, 186-201.
3. G. F. Payne and S. R. Raghavan, *Soft Matter*, **2007**, *3*, 521-527.
4. M. Bulwan, S. Zapotoczny and M. Nowakowska, *Soft Matter*, **2009**, *5*, 4726-4732.
5. L. Heux, J. Brugnerotto, J. Desbrières, F. Versali and M. Rinaudo, *Biomacromolecules*, **2000**, *1*, 746-751.
6. E. I. Kulish, R. R. Fatkullina, V. P. Volodina, L. V. Kolesov and Y. B. Monakov, *Rus. J. Appl. Chem.*, **2007**, *12*, 1178-1180.
7. E. I. Rabea, M. E.-T. Badawy, C. V. Stevens, G. Smagghe and W. Steurbauth, *Biomacromolecules*, **2003**, *4*, 1457-1465.
8. G. Cárdenas, P. Anaya, C. v. Plessing, C. Rojas and J. Sepúlveda, *J. Mater. Sci.*, **2008**, *19*, 2397-2405.
9. F. J. Pavinatto, A. Pavinatto, L. Caseli, D. S. d. Santos, T. M. Nobre and M. Zaniquelli, *Biomacromolecules*, **2007**, *8*, 1633-1640.
10. R. Shepherd, S. Reader and A. Falshaw, *Glycoconjugate Journal*, **1987**, *14*, 535-542.
11. J. Desbrières, C. Martinez and M. Rinaudo, *Int. J. Bio. Macromolecules*, **1996**, *19*, 21-28.
12. (a) Y. M. Yang, W. Hu, X. D. Wang and X. S. Gu, *J. Mater. Sci.*, **2007**, *18*, 2117-2121; (b) N. Roy, N. Saha, T. Kitano and P. Saha, *Soft Materials*, **2010**, *8*, 130-148.
13. F. S. Ligler, B. M. Lingerfelt, R. P. Price and P. E. Schoen, *Langmuir*, **2001**, *17*, 5082-5084.
14. T. Dvir, B. P. Timko, D. S. Kohane and R. Langer, *Nat. Nanotech.*, **2011**, *6*, 13-22.
15. Y. Ohshima, K. Nishino, Y. Yonekura, S. Kishimoto and S. Wakabayashi, *Eur. J. Plast. Surg.* , **1987**, *10*, 66.
16. R. H. Chen, W. Y. Chen, S. T. Wang, C. H. Hsu and M. L. Tsai, *Carbohydr. Polym.*, **2009**, *78*, 902-907.
17. K. M. Gray, E. Kim, L.-Q. Wu, Y. Liu, W. E. Bentley and G. F. Payne, *Soft Matter*, **2011**, *7*, 9601-9615.
18. C. M. Valmikinathan, V. J. Mukhatyar, A. Jain, L. Karumbaiah, M. Dasari and R. V. Bellamkonda, *Soft Matter*, **2012**, *8*, 1964-1976.
19. ASTM E 2149–01, Standard Test Method for Determinating the Antimicrobial Activity of Immobilized Antimicrobial Agents under Dynamic Contact Conditions.
20. S. L. Buckhout-White and G. W. Rubloff, *Soft Matter*, **2009**, *5*, 3677-3681.
21. M. Pereda, M. I. Aranguren and N. E. Marcovich, *J. Appl. Polym. Sci.*, **2008**, *107*, 1080-1090.
22. Z. Osman and K. Arof, *Electrochim. Acta*, **2003**, *42*, 993-999.
23. E. A. El-Hefian, M. M. Nasef, A. H. Yahaya and R. A. Khan, *J. Chil. Chem. Soc.* , **2010**, *1*, 130-136.
24. J. Li, Y. Du and H. Liang, *Polymer Degradation and Stability*, **2007**, *92*, 515-524.
25. G. C. Ritthidej, T. Phaechamud and T. Koizumi, *Int. J. Pharmaceutics*, **2007**, *232*, 11-22.
26. N. Bhattarai, H. R. Ramay, S. H. Chou and M. Zhang, *Int. J. Nanomedicine*, **2006**, *1*, 181-187.
27. W. Weecharangsan, P. Opanasopit, T. Ngawhirunpat, T. Rojanarata and A. Apirakaramwong, *AAPS Pharmaceutica* **2006**, *7*, E74-E79.

28. Y. Li, X. G. Cheng, N. Liu, C. S. Liu, C. G. Liu and X. H. Meng, *Carbohydrate Polymers*, **2007**, *67*, 227-232.
29. H. Saito, R. Tabeta and K. Ogawa, *Macromolecules*, **1987**, *20*, 2424-2430.
30. K. V. H. Prashanth, F. S. Kittur and R. N. Tharanathan, *Carbohydrate Polymers*, **2002**, *50*, 27-30.
31. H. Saito, S. Tuzi and A. Naito, in *Solid State NMR of Polymers: Polisaccharide and Biological Systems*, eds. I. Ando and T. Asakura, Elsevier, Tokyo, Japan, 1998, pp. 891-921.
32. J. Nunthanid, S. Puttipipatkhachorn, K. Yamamoto and G. Peck, *Drug Dev. Ind. Pharm.*, **2001**, *27*, 143-157.
33. B. G. Amsden, A. Sukarto, D. K. Knight and S. N. Shapka, *Biomacromolecules*, **2007**, *8*, 3758-3766.
34. S. Zivanovic, S. Chi and A. Draughon, *J. Food Sci.*, **2005**, *70*, 45-51.
35. M. Rinaudo, *Prog. Polym. Sci.* , 2006, **31**, 603-632.
36. F. L. Mi, Y. B. Wu, S. S. Shyu, J. Y. Schoung, Y. B. Huang and Y. H. Tsai, *J. Biomed. Mater. Res.*, **2002**, *59*, 438-449.
37. S. Zivanovic, J. Li, M. Davidson and K. Kit, *Biomacromolecules*, **2007**, *8*, 1505-1510.
38. L. J. R. Foster and J. Butt, *Biotechnol. Lett.*, **2011**, *33*, 417-421.
39. N. Bhattarai, J. Gunn, M. Zhang, *Adv. Drug Deliv. Rev.* **2010**, *62***,** 83-99.
40. T. Kean, M. Thanou, *Adv. Drug. Deliv Rev.* **2010**, *62***,** 3-11.
41. R. A. A. Muzzarelli, *Cell. Mol. Life Sci.*, **1997**, *53*, 131-140.
42. K. Tomihata and Y. Ikada, *Biomaterials*, **1997**, *18*, 567-575.
43. T. Freier, H. Koh, K. Kazazian and M. Shoichet, *Biomaterials*, **2005**, *26*, 5872-5878.
44. Lysozyme was continually refreshed every few days during the tests.
45. R. Nordtveit, K. M. Varum and O. Smidsrod, *Carbohydr. Polym.* , **1994**, *23*, 253-260.

TABLE 1. Variables and levels for the experimental designs. Compounds in italics are secondary additives in each experimental design.

Variable		**Level**	
Experimental design A 64 samples Labels: 1001-1064	I: chitosan molecular weight	68 k	138 k
	II: chitosan percentage (% p/v)	1	2
	III: solvent	acetic acid	lactic acid
	IV: glycerol (%v/v)	0.25	0.50
	V: oleic acid (% v/v)	0	0.003
	VI: linoleic acid (% v/v)	0	0.005
Experimental design B 32 samples Labels: 2001-2032	I: chitosan molecular weight	68 k	263 k
	II: chitosan percentage (% p/v)	1	2
	III: solvent	acetic acid	lactic acid
	IV: glycerol (% v/v)	0.25	0.50
	VII: tween 20 (% v/v)	0.010	0.250
Experimental design C 32 samples Labels: 8001-8032	I: chitosan molecular weight	68 k	263 k
	II: chitosan percentage (% p/v)	1	2
	III: solvent	acetic acid	lactic acid
	IV: glycerol (% v/v)	0.25	0.50
	VIII: tween 80 (% v/v)	0.010	0.250

TABLE 2. Independent variables employed in the experimental designs.

Variable	**Code**	
Principal	Chitosan molecular weight	I
	Chitosan percentage	II
	Solvent	III
	Glycerol	IV
Secondary	*Oleic acid*	V
	Linoleic acid	VI
	Tween 20	VII
	Tween 80	VIII

TABLE 3. Microorganisms employed for the antimicrobial assays.

Type	Name	ATCC code
Gram positive bacteria	*Staphylococcus aureus*	ATCC 6538
	Staphylococcus epidermidis	ATCC 12228
	Streptococcus pyogenes	ATCC 19615
	Bacillus subtilis	ATCC 6633
Gram negative bacteria	*Escherichia coli*	ATCC 9637
	Pseudomona aeruginosa	ATCC 9027
	Acinetobacter baumannii	ATCC 19606
	Klebsiella pneumoniae	ATCC 10031
	Salmonella spp.	ATCC 14028
	Enterobacter spp.	ATCC 13048

TABLE 4. FTIR vibrational modes of powders and cast gel films. The band at 1560 cm^{-1} is assigned to the N-H bending (amide I) (NH_2) while the small peak at 1651 cm^{-1} is attributed to the C=O stretching (amide I) O=C-NHR. Bands at 2917, 2866, 1432, and 1251 cm^{-1} are assigned to CH_2 bending due to the pyranose ring, while CH_3 wagging vibrations are located at 1379 and 1323 cm^{-1}. The band from amide type III is seen at 1323 cm^{-1}, due to the combination of N-H deformation and the C-N stretching vibration. A band at 1028 cm^{-1} due to C-O stretching of C6 from chitosan (primary OH) and at 1089 cm^{-1} from the symmetric stretching of C-O-C, are also observed. The asymmetric stretching of C-O-C appears at 1157 cm^{-1}, and a small C-C band at 895 cm^{-1} is also found.

	Absorption (cm^{-1})											
Sample	$\nu_{C=O}$ **lactic acid**	$\nu_{C=C}$	$\nu_{C=O}$ **Amide I**	δ_{NH2} **Free amine**	δ_{NH3}^{+} + ν_{COO}^{-} **chitosan salt**	δ_{CH2} δ_{CH3} and δ_{C-CH3}	ν_{COO}^{-} **acids**	δ_{NH} + ν_{C-N}	ν_{C-O}	ν_{C-O} **glycerol and/or acids**	$\nu^{as}{}_{C-O-C}$ **ring**	δ_{CO-OH} **acids**
Chitosan			1655	1598		1424 and 1381		1330	1253, 1091 and 1025		1153	

1001			1632		1568	1420 and 1375	1412	1337	1259, 1087	1050	1159	924
1033			1639	1593	1554	1421 and 1378	1412	1340	1262	1046	1153	927
1035		1695 and 646			1580	1420	1420	1335	1250, 1095 and 1014	1040	1152	925
1043	1728	683			1557	1451	1416	1311	1259	1030	1149	921
2006	1734				1567	1425 and 1378	1411	1332	1254	1052	1146	951
2017			1639		1569	1380	1412	1335	1256, 1093 and 1027	1027	1151	936
2021	1730				1580	1372	1414	1314	1267, 1092 and 1024	1067	1146	948
8004	1735				1567	1460	1408	1338	1254, 1096 and 1024	1034	1146	945
8017		1683 and 646			1573	1420	1413	1334	1261, 1093	1034	1153	925
8021	1731	659			1581	1454 and 1375	1412	1314	1250, 1085	1037	1123	926
8030	1732	659			1570	1454 and 1375	1414	1311	1258, 1083	1027	1119	948

TABLE 5. Chemical shifts from ^{13}C / CP-MAS of the chitosan composites.

	Chemical Shift (ppm)						
Carbon assigned	***Chitosan*[1]**	***Chitosan*[2]**	***Chitosan acetate*[3]**	***Chitosan acetate*[4]**	***1001***	***8026***	***8030***
C=O (carboxylate)	ND[5]	ND[5]	181.1	180.6	181.1	181.4	183.7

C=O (chitosan)	ND[5]	174.6	174.3	ND[5]	ND[5]	ND[5]	ND[5]
C_4	104.7	104.2	102.4	98 – 102.3	105.1	104.2	100.0
C_3	81.0 – 85.7	83.4	82	82	84.4	80.2	ND[5]
C_5	74.1	75	76.2	77	74.9	74.7	75.8
C_5	74.1	75	76.2	73	74.9	74.7	71.2
C_6	59.6 – 60.7	61	60	60	60.5 – 62.9	57.0	56.1
C_2	56.8	56.6	60	57	57.02	57.0	56.1
CH_3 (chitosan)	ND[5]	24.06	24	ND[5]	ND[5]	ND[5]	ND[5]
CH_3 (carboxylate)	ND[5]	ND[5]	25.1	25.2	24.5	24.6	21.0

[1] Chitosan, GD = 100%

[2] Chitosan, GD = 82%

[3] Chitosan acetate, GD = 82%

[4] Chitosan acetate, GD = 100%

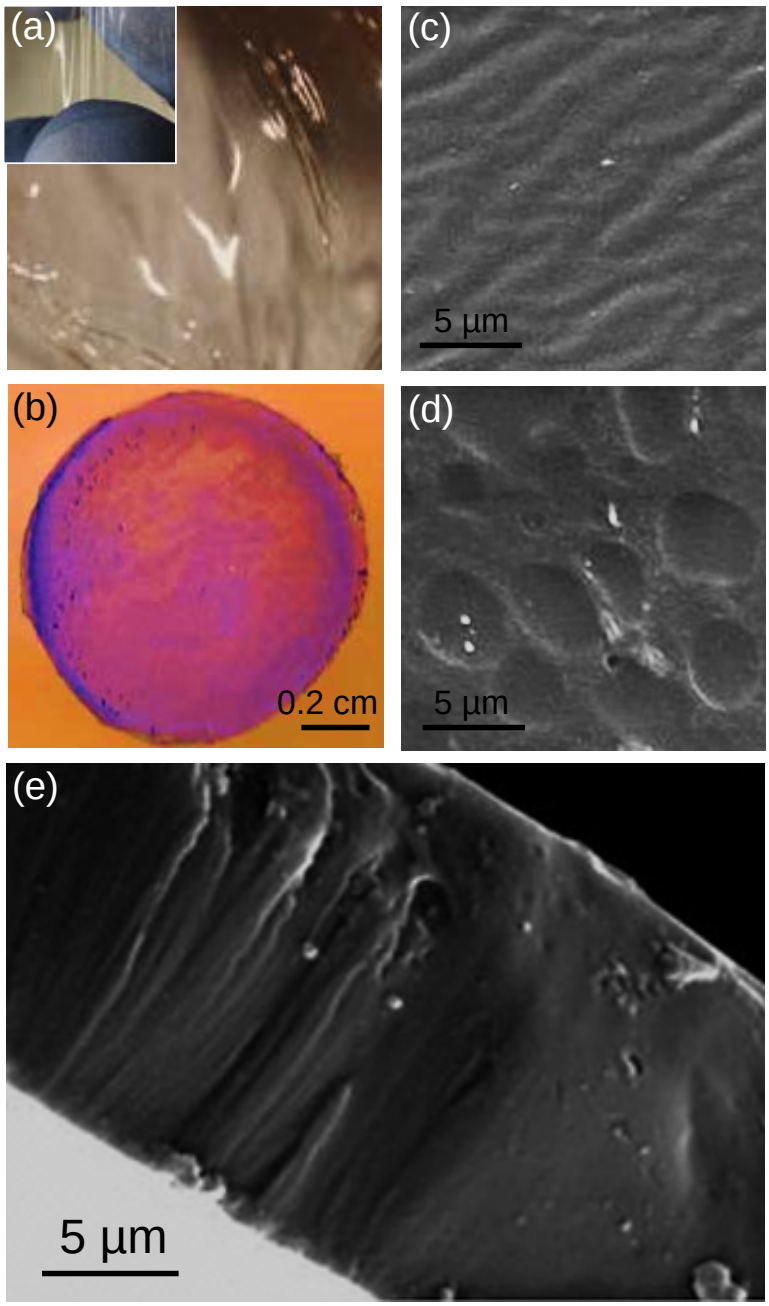

FIGURE 1. (a) Optical micrograph of a chitosan acetate film and a fully formed chitosan lactate gel film. (b) Differential interference contrast optical image of a chitosan lactate and glycerol gel film disc. (c) SEM image of the surface of a gel film of chitosan lactate with glycerol and (d) of chitosan lactate with glycerol and tween 80. (e) Cross-sectional SEM image of a film of chitosan lactate with glycerol.

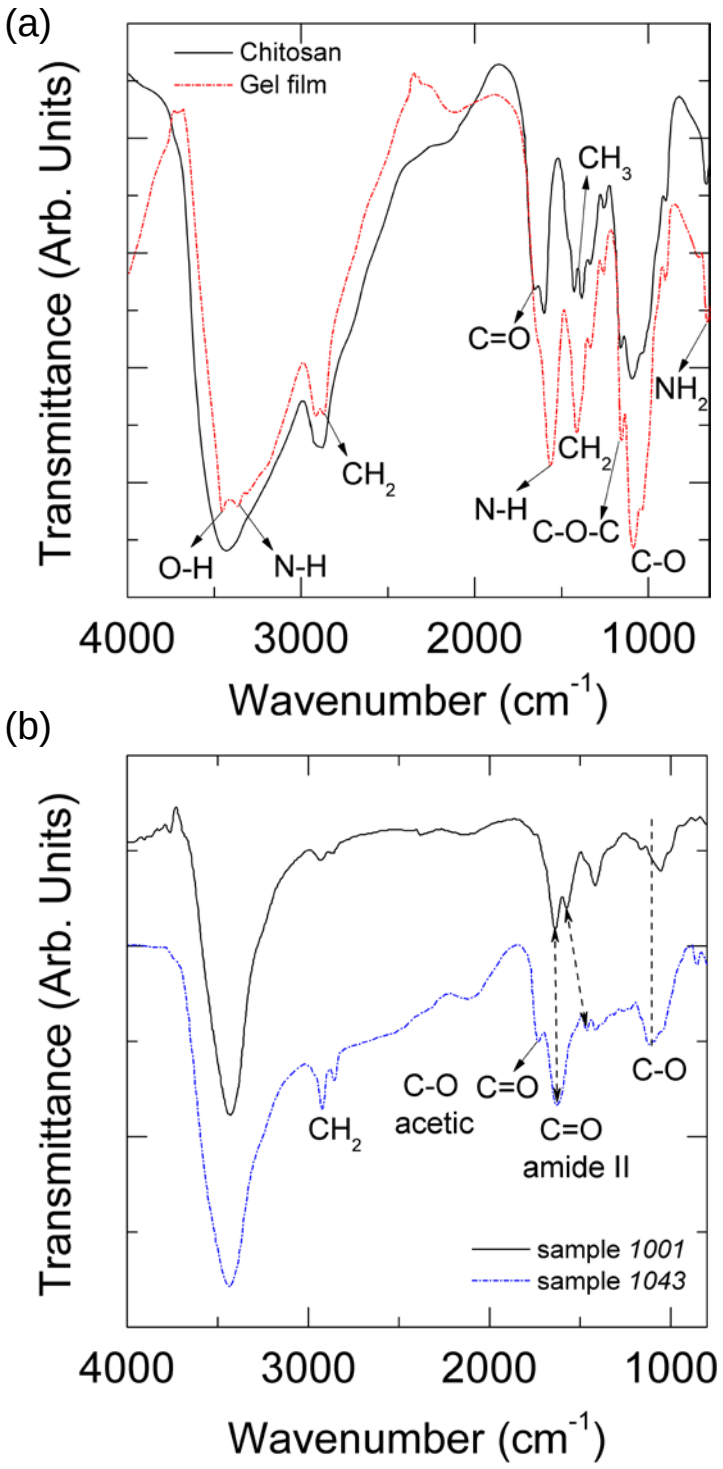

FIGURE 2. FT-IR spectrum of (a) chitosan powder and chitosan acetate and (b) chitosan composites *1001* and *1043* prepared according to Experimental Design A.

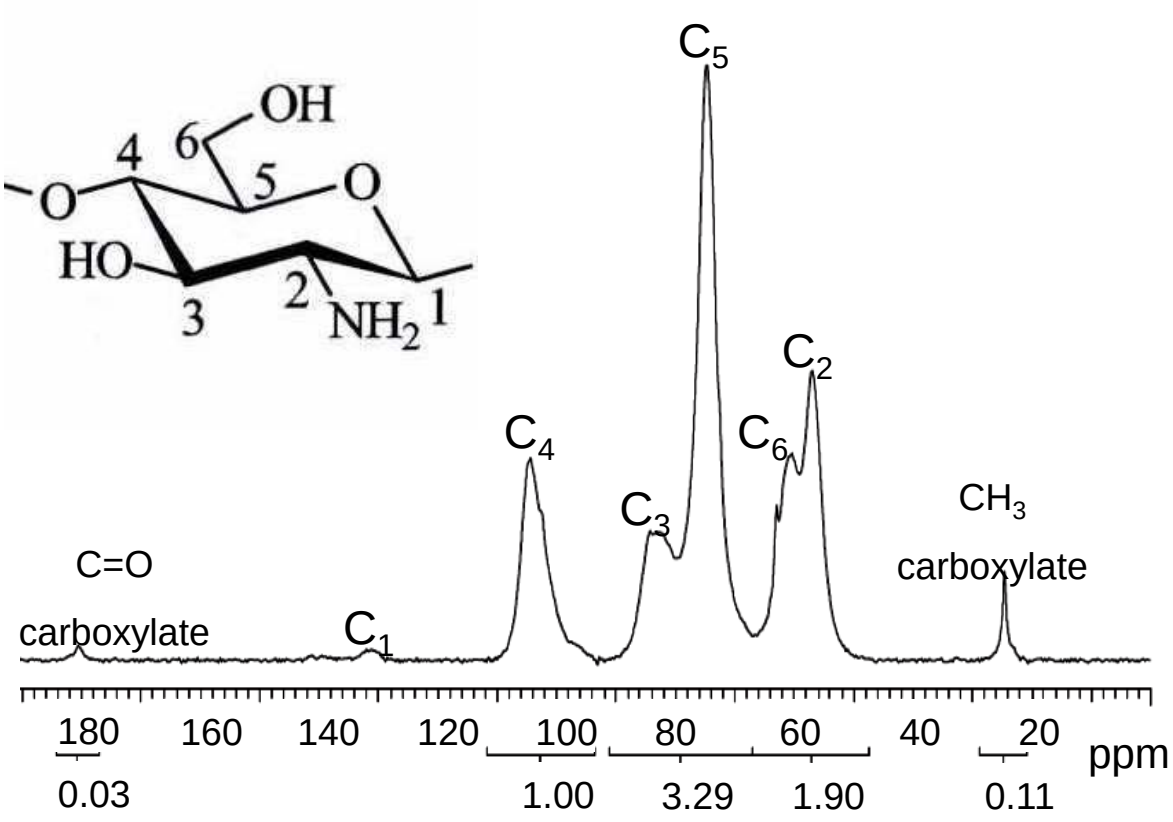

FIGURE 3. ^{13}C CP-MAS NMR spectrum of gel film *1001*.

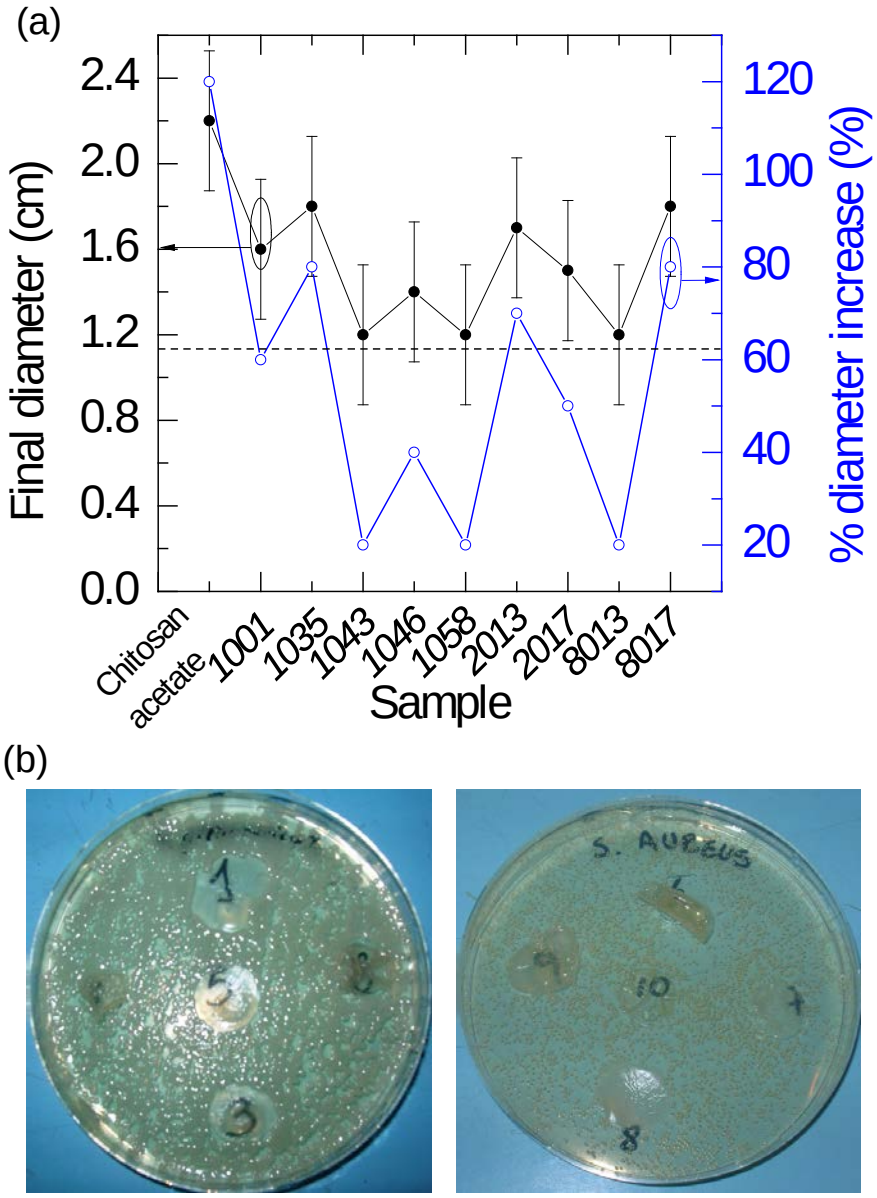

FIGURE 4. (a) Diffusion disc results of chitosan composite films and (b) inhibition halo formation, against *Klebsiella pneumonia* (left) and *Staphylococcus aureus* (right). Films that were case without plasticizing additives are more difficult to manipulate and had a tendency to roll into a tubular shape after being added to the serum and such films exhibited the greatest dimensional change due to swelling.

TABLE 3. Inhibitory effect of chitosan composite films over micro-organism growth under dynamic conditions.

	Number of survival microorganisms (CFU/mL)			
Sample	*S. aureus*	*S. epidermidis*	*P. aeruginosa*	*K. pneumoniae*
Control	1.6×10^6	5.5×10^5	1×10^8 [a]	1×10^8 [a]
Chitosan acetate	1×10^2	0	6×10^1	1×10^2
1043	0	8×10^1	0	1×10^1
1058	1.5×10^2	0	3×10^1	2×10^1
2013	0	3×10^1	1×10^1	3×10^1
8017	1×10^1	1×10^8 [a]	1×10^2	1×10^2

[a] It was not possible to accurately count the number of colonies; an average of 1×10^8 CFU/mL was determined.

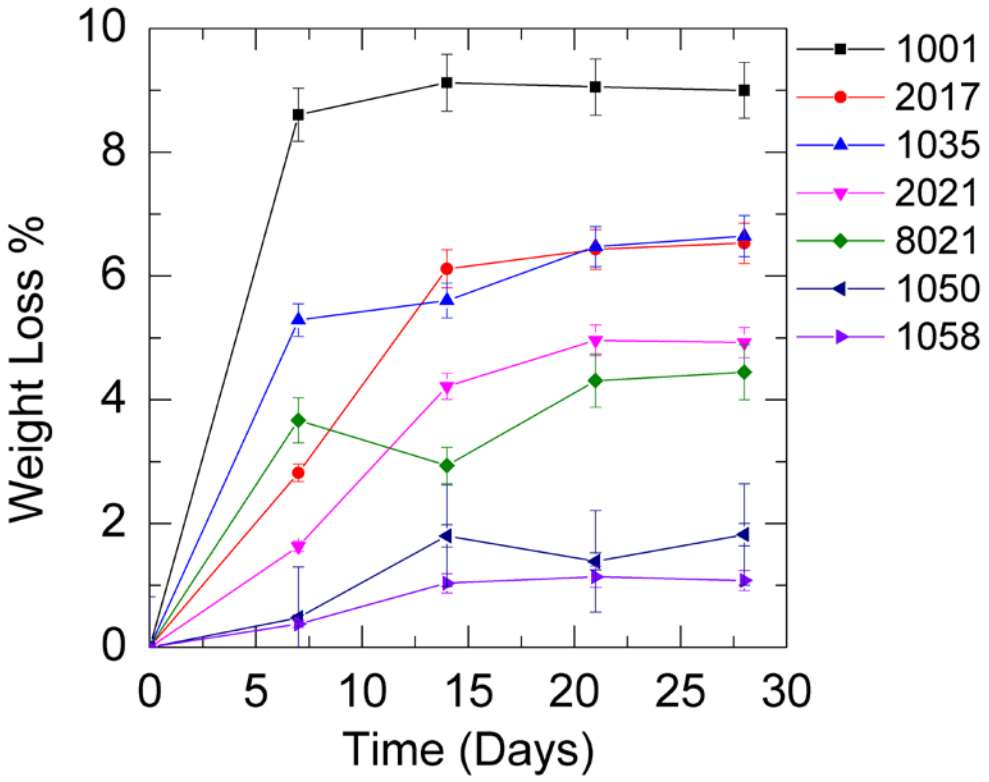

FIGURE 5. Standardized weight loss for 8 composites from all Experimental Design series under *C1* assay.

GRAPHICAL FIGURE